

## Sequential resonant tunneling characteristics of AlAs/GaAs multiple-quantum-well structures

S. Tarucha\* and K. Ploog

*Max-Planck-Institut für Festkörperforschung, D-7000 Stuttgart 80, Federal Republic of Germany*

(Received 23 December 1987)

The resonant tunneling characteristics of AlAs/GaAs multiple-quantum-well structures are studied using time-resolved photocurrent (PC) as well as static PC and photoluminescence measurements. The high potential barrier formed by AlAs allows one to observe resonant tunneling from the ground state ( $1e$ ) in one well to the first three excited states ( $2e$ ,  $3e$ , and  $4e$ ) in the neighboring well. Pronounced features due to resonant tunneling are observed up to temperatures as high as 260 K. The time-resolved photocurrent exhibits an enhancement of the initial decay under the resonance of electrons. The resonant tunneling times from  $1e$  to  $3e$  and to  $4e$  are derived from the time-resolved photocurrent by using the rate equation of electron transport for a complete sequence of resonant tunneling followed by back-relaxation to  $1e$ . The tunneling times obtained are shorter by a factor of 15 to 20 than the values derived from the theory of tunneling through a single barrier.

### I. INTRODUCTION

Since the first proposal of resonant tunneling (RT) in heterostructure superlattices by Esaki and Tsu,<sup>1</sup> this subject has been considered one of the most essential characteristics of vertical transport properties in superlattices and multiple-quantum-well structures (MQWS). So far, most of the RT features in semiconductor superlattices have been exemplified by the observation of negative differential resistance<sup>2,3</sup> and of oscillatory conductance<sup>4</sup> in the static current-voltage ( $I$ - $V$ ) characteristics, and it is generally assumed that RT is associated with minibands in the superlattices. Resonant tunneling involving the ground state of the quantum wells is forbidden when the magnitude of the bias voltage per superlattice period applied perpendicular to the layers is larger than the miniband width of the ground state. However, RT becomes again possible from the ground state in one well to the excited state in the next well when the ground state becomes approximately degenerate with the excited state by applying a further increased bias voltage. This feature of resonant tunneling was originally proposed by Kazari-nov and Suris,<sup>5</sup> and later exemplified by the observation of peaks in the static photocurrent-voltage characteristics of an  $\text{Al}_x\text{In}_{1-x}\text{As}/\text{Ga}_x\text{In}_{1-x}\text{As}$  MQWS (Ref. 6) and an  $\text{Al}_x\text{Ga}_{1-x}\text{As}/\text{GaAs}$  MQWS.<sup>7</sup> These photocurrent (PC) peaks indicate that the photocurrent is enhanced by the resonant tunneling of electrons from the ground state ( $1e$ ) in one well to the excited state ( $2e$ ,  $3e$ , etc.) in the neighboring well. However, as yet, only a few studies have been reported on the dynamics of resonant tunneling. Recently, time-resolved photoluminescence (PL) techniques were employed to investigate the dynamical features of RT associated with the ground state in an  $\text{Al}_x\text{Ga}_{1-x}\text{As}/\text{GaAs}$  MQWS (Ref. 8) and in an AlAs/GaAs double-barrier structure.<sup>9</sup> We have recently also studied the time-resolved PC as well as the static PC and PL characteristics of an  $\text{Al}_x\text{Ga}_{1-x}\text{As}/\text{GaAs}$  MQWS at low temperatures. We observed a reduction of the tun-

neling time and a PL quenching, both of which are induced by RT from  $1e$  to  $2e$  and  $3e$  in the respective adjacent wells.<sup>10</sup> The present paper describes a detailed study of the resonant-tunneling characteristics associated with the ground and excited states in the adjacent respective wells observed in an AlAs/GaAs MQWS. After resonant tunneling from  $1e$  in one well to  $2e$  ( $3e$ ,  $4e$ , etc.) in the next well an electron relaxes either back to  $1e$  in that next well due to phonon scattering or it tunnels out of the MQWS. The first RT feature is anticipated to be more probable in a MQWS with high-potential barriers under relatively low electric fields, while the second one is more likely for a MQWS with low potential barriers under high electric fields. The AlAs/GaAs heterostructure of the present study is expected to allow the completion of a sequence of RT followed by back-relaxation because of the high potential barriers formed by AlAs. In addition, RT associated with the higher excited states should be feasible. These RT features in an AlAs/GaAs MQWS are studied using time-resolved PC and static PC and PL measurements. The tunneling times of electrons from  $1e$  to  $3e$  and  $4e$  in the respective adjacent wells are derived from the detailed analysis of the time-resolved PC using a rate equation for electron transport. Weak-excitation conditions are employed to minimize the space-charge effect induced by the photogenerated carriers and the exciting energy is adjusted to create carriers homogeneously in the MQWS along the axis of the layer sequence.

### II. SAMPLE PREPARATION AND EXPERIMENTAL SETUP

The sample is a  $p$ - $i$ - $n$  heterostructure diode grown by molecular beam epitaxy (MBE). The intrinsic region consists of a 50-period AlAs(3.4 nm)/GaAs(14 nm) MQWS sandwiched by undoped 30-nm GaAs layers. The  $p$  and  $n$  layers are  $\text{Al}_{0.5}\text{Ga}_{0.5}\text{As}$  ( $0.8 \mu\text{m}$ ,  $n=p=5 \times 10^{17} \text{ cm}^{-3}$ ) with graded  $\text{Al}_x\text{Ga}_{1-x}\text{As}$  regions next to the MQWS. The diode is processed into a high-mesa cylindrical

geometry having a diameter of 200  $\mu\text{m}$ . The built-in voltage of the diode is 1.6 V at 10 K, as evaluated from the PC-voltage characteristics. The breakdown voltage at reverse bias is above 20 V at 10 K, and the dark current is less than  $10^{-9}$  A. The cutoff frequency derived from the RC time constant is about 5 GHz. The time-resolved PC is measured using a 785-nm  $\text{Al}_x\text{Ga}_{1-x}\text{As}$  double-heterostructure laser diode as exciting light source. Optical pulses of 350-ps duration and 100-kHz repetition rate are generated by injecting electrical pulses into the laser diode. The optical pulse has a Lorentzian-like time profile. The absorption coefficient is about 0.02 per well at 785 nm.<sup>11</sup> The density of photogenerated carriers is  $1 \times 10^{14} \text{ cm}^{-3}$  per pulse. The other details of the experimental setup are the same as described previously.<sup>10</sup>

### III. STATIC PHOTOLUMINESCENCE AND PHOTOCURRENT CHARACTERISTICS

Figure 1 shows the static PC and the spectrally integrated PL intensity as a function of the bias voltage ( $V_b$ ) measured under the same cw excitation conditions. The 753-nm line of a  $\text{Kr}^+$  laser with  $0.3 \text{ W/cm}^2$  is used as exciting light source. The negative sign of  $V_b$  denotes the backward of the diode. The observed PL is associated with excitons of electrons and heavy holes in the ground states. The PC shows four peaks labeled *a*, *b*, *c*, and *d*. At the same voltages where the peaks *b* and *c* appear, the PL intensity shows pronounced dips, labeled *B* and *C*, and also a complete quenching as  $V_b$  is decreased down to the value where peak *d* appears. This correspondence indicates that peaks *b*, *c*, and *d* are induced by the carriers generated by the field ionization of excitons and are therefore associated with the escape of electrons or heavy holes in the ground states from the well. We assign these PC peaks *b*, *c*, and *d* to RT of electrons from  $1e$  in one well to  $2e$ ,  $3e$ , and  $4e$  in the next well, respectively, according to the analysis of the corresponding electric fields. The electric fields across each constituent MQWS

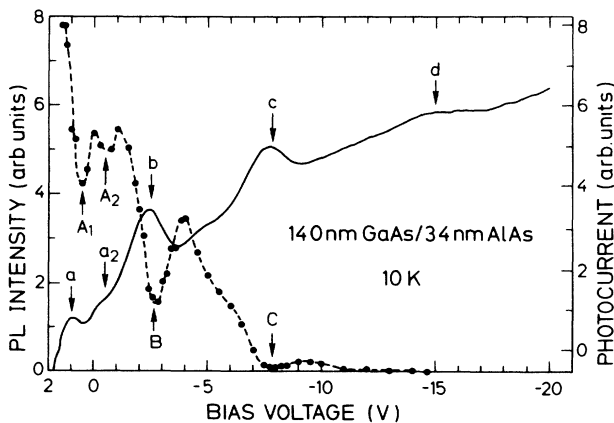


FIG. 1. Static photocurrent (solid line) and spectrally integrated photoluminescence intensity (solid circles) vs bias voltage measured under the same cw excitation condition. The dashed line along the solid circles is a guide for the eyes.

are determined from the  $\text{PC}/V_b$  characteristics at sufficiently low excitation intensity in order to eliminate the field-screening effect by the photogenerated carriers. The obtained voltages are  $-2.4$ ,  $-7.5$ , and  $-13.8$  V for the peaks *b*, *c*, and *d*, respectively, which are invariant within an error of 0.2 V below  $20 \text{ mW/cm}^2$ . These values give the electric fields of 43, 98, and 165 kV/cm, respectively. The effective-mass calculation, on the other hand, gives the subband energy differences of 63 meV between  $1e$  and  $2e$ , 163 meV between  $1e$  and  $3e$ , and 296 meV between  $1e$  and  $4e$ , respectively. These values predict RT of electrons at 36, 94, and 170 kV/cm, which agree well with those for peaks *b*, *c*, and *d*, respectively.<sup>12</sup> The RT features occurring at these electric fields are further confirmed by the time-resolved PC measurements described later. It is important to note that the observation of RT even from  $1e$  to  $4e$  proves the confinement of electrons by the  $\Gamma$  band of the AlAs barrier, not by the  $X$  band. The PC peak *a* and the PL dip  $A_1$  are probably due to the field-induced change of the absorption coefficient at the exciting energy because peak *a* is not observed under white-light excitation (see Fig. 4). In addition, the dip  $A_1$  accompanies a PC dip at the same voltage. The small PL intensity dip  $A_2$  accompanies a small excess PC indicated by  $a_2$ . Their origin is not yet well understood.

The PL spectral change around the voltages providing the PL quenchantings (dips *B* and *C*) are shown in detail in Fig. 2. The inset shows the PL emission energy as a function of  $V_b$  as determined by the arrows. When  $V_b$  is decreased, the PL shifts to lower energies and is accompanied by a spectral broadening. The latter is probably due to the monolayer fluctuation of the well size.<sup>13</sup> The

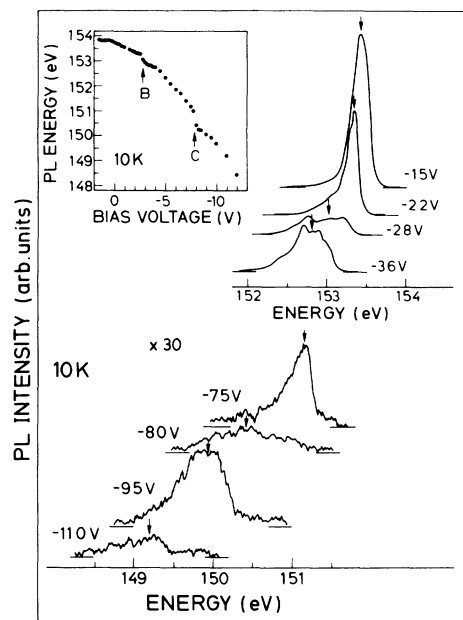


FIG. 2. Spectral change of photoluminescence around the bias voltage  $V_b$  from  $-1.5$  to  $-3.5$  V (upper part) and from  $-7.5$  to  $-11.0$  V (lower part). The inset shows the PL emission energy vs  $V_b$  as determined by the arrows.

observed Stark shift is smaller than the calculated value even when the field screening by the photogenerated carriers is taken into account. This small Stark shift is qualitatively explained by the large confinement of the AlAs barriers, but quantitatively it is not yet understood.<sup>14</sup> Of particular interest is that the Stark shift shows an irregularity around the voltages corresponding to the PL quenched regions (dips *B* and *C*), although it is otherwise proportional to the square of the electric field as a general shift in the whole  $V_b$  range. We attribute the irregularity to the spectral inhomogeneity in the PL quenching, which is caused by two possible phenomena, i.e., intralayer fluctuation of the well size and inhomogeneity of the electric field. First, the monolayer fluctuation of the well size is inevitable in conventional MBE growth. The excitons are localized by the intralayer fluctuation whose lateral dimension is larger than the exciton Bohr diameter. The recombination of excitons localized in the wider well region provides luminescence in the lower energy range because of the smaller confinement. The subband energy spacing is also smaller for the wider well. This means that PL associated with the wider well, which forms the low-energy side of the whole PL spectrum observed, is quenched by RT at the lower electric field. This mechanism is actually proven by a detailed analysis of the spectra. Figure 3 shows the distinct change of the PL spectrum as  $V_b$  is decreased toward the value providing dip *B*. The spectrum shows a fine structure as indicated by arrows 1 and 2, which is due to the one-monolayer fluctuation of the well size. The Stark shift of the PL spectrum is determined precisely by following the fine structure. We can then compare all spectra at different  $V_b$  values after shifting each spectrum by the amount of the Stark shift. This comparison clearly reveals that the quenching extends from the low-energy side to the high-energy side as  $V_b$  is decreased. In the same way we find that the recovery of the PL intensity after the quenching also extends from the low-energy side to the high-energy side. This spectral inhomogeneity in the PL quenching results in the irregularity of the apparent Stark shift.

Second, an inhomogeneity of the electric field across

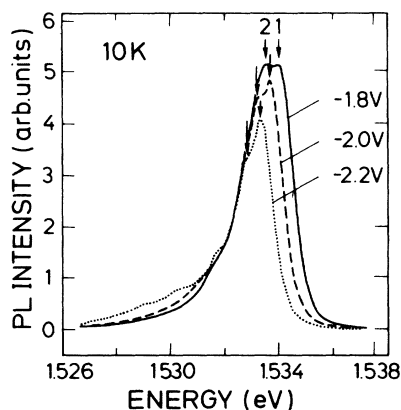


FIG. 3. Detailed spectral change of photoluminescence around bias voltage  $V_b$  from  $-1.8$  to  $-2.2$  V.

the MQWS is induced by the space charge, which is mainly associated with background impurities (the acceptor concentration is  $p < 10^{15} \text{ cm}^{-3}$ ). Any space charge associated with the photogenerated carriers can be neglected for the low excitation employed here. The space charge makes the field higher in the region of the MQWS closer to the *n* region of the diode. The recombination of excitons in these wells under the higher electric field, which forms the low-energy side of the whole PL spectrum because of the larger Stark shift, is quenched under a lower external electric field as  $V_b$  is decreased toward the value providing RT. This mechanism is also able to induce a spectral inhomogeneity of the PL quenching induced by RT, although it is not yet experimentally confirmed.

Figure 4 shows the temperature dependence of the observed photocurrent versus bias voltage characteristics. In this case white-light excitation is used to eliminate the field-induced change of the absorption coefficient. The excitation intensity is  $20 \text{ mW/cm}^2$  or less. The important result of these measurements is that the PC peaks *b* and *c* due to RT between  $1e$  and  $2e$  and between  $1e$  and  $3e$ , respectively, are observed up to temperatures as high as 260 K. Most of the previous observations of RT in MQWS's were achieved only at low temperatures: below 50 K for the  $\text{Al}_x\text{In}_{1-x}\text{As}/\text{Ga}_x\text{In}_{1-x}\text{As}$  MQWS (Ref. 6) and below 77 K for the  $\text{Al}_x\text{Ga}_{1-x}\text{As}/\text{GaAs}$  MQWS's.<sup>7,10</sup> This result implies the existence of well-defined subband levels formed by the high potential barriers and also a high crystal quality. As the temperature is increased, the PC becomes smaller up to temperatures of 120 K and then larger again. In addition, shoulderlike features labeled *b*<sub>1</sub> and *b*<sub>2</sub> become more pronounced at higher temperatures. The observed increase of the PC above 120 K is attributed to phonon-assisted tunneling. In particular, the shoulderlike features indicate a field-induced enhancement of LO-phonon-assisted tunneling because the voltage difference between peak *b* and features *b*<sub>1</sub> and *b*<sub>2</sub> gives a potential drop across the MQW period in the range of 30 to 40 meV, which is comparable to the LO-phonon energy in GaAs. This assignment is more likely for the feature *b*<sub>2</sub> because of the larger probability for phonon emission than for phonon absorption. The de-

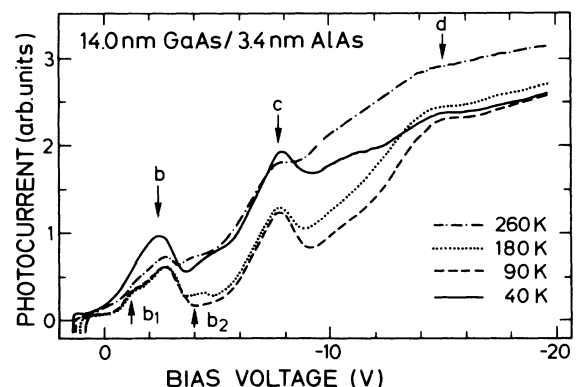


FIG. 4. Static photocurrent vs bias voltage measured at different temperatures.

crease of PC below 120 K is attributed to thermally activated nonradiative centers because the PL intensity is also reduced in this temperature range. Defects or impurities at the heterointerfaces or in the AlAs barriers are a possible origin for these nonradiative centers. The PC peaks *b* and *c* are not significantly distorted with increasing temperatures up to 180 K. The features become broader above 180 K which indicates that the trapping time of any nonradiative centers is longer than the escape time of electrons out of the entire MQWS under resonance in the temperature range from 10 to 180 K.

#### IV. TIME-RESOLVED PHOTOCURRENT CHARACTERISTICS

The dynamical features associated with RT are next investigated in detail using time-resolved PC measurements, which reflect the RT features more directly than the static characteristics.<sup>10</sup> The time-resolved PC observed around  $V_b$  providing RT from  $1e$  to  $2e$ ,  $3e$ , and  $4e$  is shown in Fig. 5. The time-resolved features are observable for the bias-voltage range  $V_b < -0.8$  V because of the limitation imposed by the signal-to-noise ratio. When the voltage  $V_b$  approaches the value giving the resonance, the initial decay becomes larger. The peak (maximum) value of the time-resolved PC (PCM) is plotted as a function of  $V_b$  in Fig. 6. These data clearly show that PCM reaches a peak around  $-2.5$ ,  $-7.9$ , and  $-14.85$  V. These  $V_b$  values agree well with those corresponding to the PC peaks *b*, *c*, and *d*, respectively, in Fig. 1. The ob-

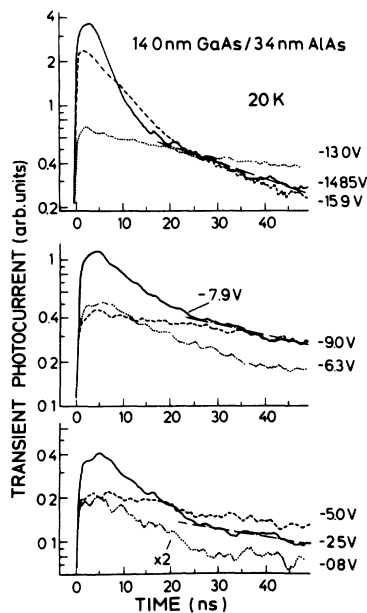


FIG. 5. Time-resolved photocurrent around the bias voltages giving resonant tunneling from  $1e$  to  $2e$  ( $-2.5$  V), from  $1e$  to  $3e$  ( $-7.9$  V), and from  $1e$  to  $4e$  ( $-14.85$  V).

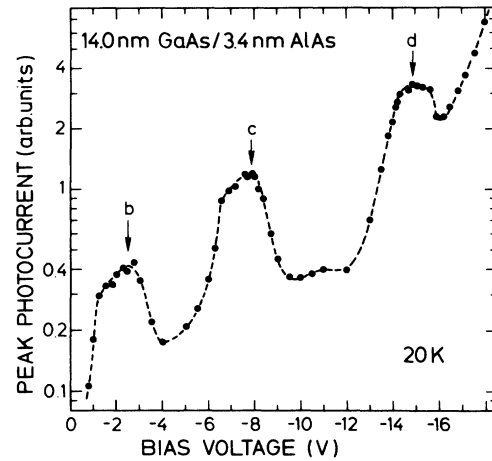


FIG. 6. Peak (maximum) value of the time-resolved PC (PCM) as a function of bias voltage  $V_b$ .

served  $V_b$  dependence of the time-resolved PC confirms that the escape time of electrons from the entire MQWS is reduced by RT. The large initial decay occurs in the time range from 0 to 20 ns around  $-2.5$  V, from 0 to 20 ns around  $-7.9$  V, and from 0 to 15 ns around  $-14.85$  V. (To define the decay time of the time-resolved PC rigorously in the whole  $V_b$  range may be meaningful only to a certain extent, because of the overlap with the subsequent slow decay.) When the voltage  $V_b$  is further decreased below  $-16$  V, the initial decay becomes larger again. It becomes larger monotonously with a considerably shorter decay time. This phenomenon is probably due to the preferential breakdown of AlAs layers at higher electric fields (above  $200$  kV/cm<sup>2</sup>). The initial fast decay of the time-resolved PC under resonance is followed by a slow subsequent decay, as indicated by the dash-dotted lines in Fig. 5. The latter decay time is approximately more than one order of magnitude longer than that for the initial decay, although it is difficult to determine the decay time precisely in the present measuring time scale. We assume two reasons for this subsequent slow decay. One is the trapping of electrons by the localized states formed by the fluctuation of the well size and also by the space charge, whose origins are explained before. The other is the vertical transport associated with the heavy holes, which is expected to be slower than that of electrons because of the larger confinement. The bipolar transport is extremely difficult to analyze and these contributions are not yet well understood. Therefore, in the present study, we discuss only the initial fast decay observed under resonance by assuming that it is determined by resonant tunneling of the electrons. It is quite reasonable to assume separate transport mechanisms for the initial and subsequent decays if the time scale for the transport is significantly different and if the space-charge effect induced by the charged carrier transport is neglected.<sup>15</sup> This condition holds for the present time-resolved PC under resonance. A detailed analysis of the initial decay is given in the next section.

## V. ANALYSIS OF RESONANT-TUNNELING DYNAMICS

After tunneling through one barrier an electron either relaxes back to  $1e$  of the respective well due to nonradiative phonon scattering or it tunnels out of the MQWS. These two mechanisms are competitive, depending on the values of (i) the nonradiative relaxation time of electrons from the excited state to the ground state  $\tau_f$ , (ii) the tunneling time of electrons from the excited state out of the MQWS  $\tau_v$ , and (iii) the number of wells,  $N_w$ . The resonant tunneling followed by back-relaxation becomes dominant for the ratio of  $(\tau_v/\tau_f) \gg N_w$ , while RT followed by tunneling out of the MQWS becomes dominant for the ratio  $(\tau_v/\tau_f) \ll N_w$ . Since  $\tau_f$  is in the order of  $10^{-13}$  s, RT followed by tunneling out of the MQWS becomes observable when  $\tau_v < 1 \times 10^{-11}$  s for  $N_w = 50$ . However, the decay time at which the large initial decay induced by resonance appears in the time-resolved PC, divided by  $N_w$ , is in the order of  $10^{-11}$  to  $10^{-10}$  s, i.e., much longer than  $\tau_f$ . This finding indicates that an electron after tunneling through one barrier completely relaxes back to the ground state from the excited state due to phonon scattering, i.e.,  $(\tau_v/\tau_f) \gg N_w$ , and that in addition the tunneling time is much longer than  $\tau_f$ . Therefore, only the first RT mechanism is taken into account in our analysis of the dynamics of resonant tunneling.

We apply the theory of charge transport in a perfect insulator<sup>15</sup> to analyze the observed time-resolved PC. Our MQWS is sufficiently resistive to be considered as an insulator. The basic equations to describe the charge transport are that of the total current density

$$j(t) = en(z,t)\mu F(z,t) + \epsilon \partial F(z,t) / \partial t \quad (1)$$

and the Poisson equation

$$\epsilon \partial F(z,t) / \partial z = en(z,t). \quad (2)$$

Here, we assume a one-dimensional planar electron flow along the axis  $z$  of the layer sequence and we neglect the diffusion current.  $F$  and  $n$  are the electric field and the carrier density, respectively, and  $\mu$  and  $\epsilon$  are the mobility and dielectric constant, respectively. We take  $z=0$  at the end of the MQWS neighboring the  $p$  layer and  $L [= N_w(L_z + L_B)]$  at the end neighboring the  $n$  layer, where  $L_z$  and  $L_B$  are the well thickness and the barrier thickness, respectively. The first and the second term in Eq. (1) represent the conduction and the displacement current, respectively. The total current  $j(t)$  is given by integrating Eq. (1) from  $z=0$  to  $z=L$ . For a small density of charged carriers, we assume the space-charge-free transient that  $Q(t)/\epsilon \ll F(L,t) = F(L)$ , where  $Q(t)$  is the total charge per unit area. This assumption allows to approximate the integration of Eq. (1) by

$$j(t) = \mu F(L) Q(t) / L. \quad (3)$$

The space-charge-free transient holds for the weak excitation employed here because the density of photoexcited carriers of  $1 \times 10^{14} \text{ cm}^{-3}$  gives  $Q(t)/\epsilon < 1 \text{ kV/cm}$ , which is sufficiently small as compared with the electric

field providing RT. Equation (3) means that the time dependence of the electron current is determined by  $Q(t)$ . We calculate  $Q(t)$  for a sequence of RT of electrons, as schematically shown in Fig. 7, where  $\tau_t$  and  $\tau_r$  are the tunneling time from  $1e$  in one well to  $2e$  ( $3e, 4e$ ) in the next well and the recombination time, respectively. Here,  $(\tau_v/\tau_f) \gg N_w$  and  $\tau_f \ll \tau_t$  are assumed, as described before. The electron density in the  $m$ th well  $q_m(t)$  is given by solving the rate equation

$$dq_m/dt = q_{m-1}/\tau_t - q_m/\tau_t - q_m/\tau_r. \quad (4)$$

The initial distribution of electrons is specified for impulse optical excitation as

$$q_m(0) = q_0 \exp(-\alpha m), \quad (5)$$

where  $\alpha$  is the absorption coefficient per well. The total electron density  $Q(t) = \sum_m q_m(t)$ . The electron current to be compared with the initial decay of the time-resolved PC is calculated using Eqs. (3)–(5). The value of  $\alpha = 0.02$  is assumed to be field independent.  $\tau_r$  is evaluated from time-resolved photoluminescence in the absence of an electric field, where the escape of electrons through the barriers can be neglected, and by calculating the enhancement factor under electric field.<sup>16</sup> The measured  $\tau_r$  is 3.5–4.0 ns at 20 K without electric field. We assume that this value is enhanced by about a factor of 2 at  $-2.5$  V, and by more than one order of magnitude at  $-7.9$  and  $-14.85$  V according to the field-induced spatial separation of electrons and heavy holes in the well.<sup>16</sup> The fitting of the calculated curve to the experimental data is not significantly affected by the evaluation of  $\tau_r$  for  $V_b = -7.9$  and  $-14.85$  V, as expected from Fig. 1, while it is sensitive to the evaluation of  $\tau_r$  for  $V_b = -2.5$  V. The latter is difficult to be made precisely. Therefore, we discuss extensively only the resonant tunneling observed at  $-7.9$  and  $-14.85$  V. We then assume the values  $\tau_f = 2 \times 10^{-13}$  s and  $\tau_r = 5 \times 10^{-8}$  s, both of which are not any more important parameters for the fitting to the experimental data. The fitting is carried out with  $\tau_t$  as a parameter for the initial decay of the time-resolved PC observed at  $-7.9$  V in Fig. 8(a) and at  $-14.85$  V in Fig. 8(b). The calculated curves are convoluted with the time-resolved profile of the exciting optical pulse. A good fit is achieved for  $\tau_t$  of 0.5–0.7 ns at  $-7.9$  V and of 0.23–0.28 ns at  $-14.85$  V. The fitting is better for the initial PC decay at  $-14.85$  V because of the smaller contri-

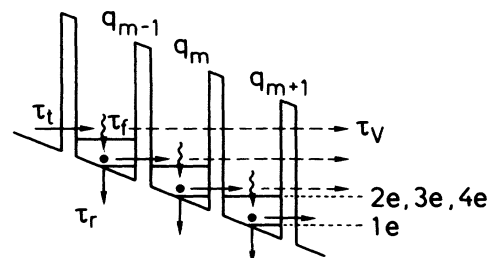


FIG. 7. Schematic diagram of resonant tunneling modeled for the calculation.

bution of the subsequent slow decay. As can be seen in Fig. 8, the calculated curve shows a linear or upper-convex decay rather than the exponential decay. This feature is more strongly reflected in the initial PC decay at  $-14.85$  V. The disagreement in the rise profile between the calculated curve and the experimental data is probably due to the effect of some inhomogeneity of the electric field across the MQWS.

The values of  $\tau_i$  obtained for RT from  $1e$  to  $3e$  and  $4e$  can be compared with theory by calculating the tunneling time using the relationship<sup>17</sup>

$$\tau_i = (2L_z/v_p)T, \quad (6)$$

where  $v_p$  and  $T$  are the phase velocity of electrons and the tunneling coefficient for a single barrier, respectively, given by

$$v_p = (\pi/L_z)(\hbar/m_1^*) \quad (7)$$

and

$$T = 16k^2\kappa^2/(k^2 + \kappa^2)\exp(-2\kappa L_B). \quad (8)$$

Here,  $k^2 = 2m_1^*E/\hbar^2$ , and  $\kappa^2 = 2m_2^*(\Delta E_c - E)/\hbar^2$ , where  $\Delta E_c$  is the conduction-band-gap discontinuity and  $E$  is the confinement energy. Under resonance  $E$  is approximated by the mean value between  $1e$  and  $3e$  ( $4e$ ). This approximation is valid when  $E \ll \Delta E_c$ , which is the case for the high potential barriers formed by AlAs. The values of  $m_1^* = 0.067$ ,  $m_2^* = 0.15$ , and  $\Delta E_c = 1.0$  eV are used for the calculation. The electrons in the ground state are confined in the triangle potential well under resonance because  $eFL_z > E$  ( $1e$ ). This effect is taken into account by assuming the effective distance of electron motion to replace  $L_z$  in Eqs. (6) and (7) by

$$L_z^* = L_z[\frac{1}{2} + E(1e)/eFL_z] \quad (9)$$

taking for granted that  $eFL_z > 2E$  ( $1e$ ). Equations (6)–(9) lead to  $\tau_i = 13$  and  $3.8$  ns for those  $V_b$  values providing RT from  $1e$  to  $3e$  and  $4e$ , respectively. The calculated tunneling time  $\tau_i$  is longer by a factor of 4–7 than the value derived from the experiment. We assume that this disagreement is due to the second-order perturbation of resonance scattering, which is not taken into account in Eq. (8). A theory which includes the effect of resonance more rigorously is required to explain the experimental value quantitatively.

The contribution of tunneling out of the MQWS's is likely to occur for MQWS with low barriers or under high electric fields. After tunneling out of the MQWS an electron reaches the  $n$ -doped region without being trapped by the wells because of the high electron mobility in the undoped AlAs/GaAs heterostructure. When the transit time is much shorter than the tunneling time through one barrier as is the case for the present MQWS, the escape time of electrons from the entire MQWS is given by  $\tau_i(\tau_v/\tau_f)$  under homogeneous excitation, where  $(\tau_v/\tau_f) < N_w/2$ . In addition, the time-resolved PC decay profile becomes more exponential-like as the ratio of  $(\tau_v/\tau_f)$  is decreased, and equivalent to that for a single QW in the limit of  $(\tau_v/\tau_f) \ll N_w/2$ .

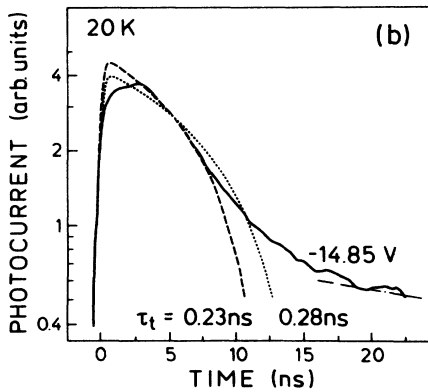
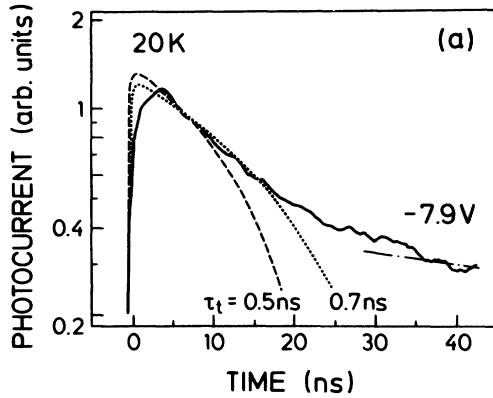


FIG. 8. Calculation of electron-induced photocurrent to be compared to the initial decay of the time-resolved photocurrent observed for resonant tunneling (a) from  $1e$  to  $3e$  and (b) from  $1e$  to  $4e$ .

## VI. CONCLUSION

The resonant-tunneling characteristics of an AlAs/GaAs MQWS were studied in detail using time-resolved PC as well as static PC and PL measurements. The high potential barrier of AlAs allows to observe RT from  $1e$  in one well to  $2e$ ,  $3e$ , and  $4e$  in the next well. The observation of RT from  $1e$  to  $4e$  proves the confinement of electrons by the  $\Gamma$  band of AlAs. Pronounced features due to RT are observed in the static photocurrent versus bias voltage characteristics even at temperatures as high as 260 K. These features of resonant tunneling imply the existence of well-defined subband levels formed by AlAs as well as an excellent crystal quality. The time-resolved photocurrent exhibits a pronounced enhancement of the initial decay under the resonance of electrons. The resonant-tunneling times from  $1e$  to  $3e$  and  $4e$  are derived

from the observed time-resolved photocurrent using the rate equation of electron transport for a complete sequence of resonant tunneling followed by back-relaxation to  $1e$ . The obtained tunneling times of 0.5–0.7 ns and 0.23–0.28 ns, respectively, are shorter by a factor of 15–20 than the values derived from the theory of tunneling through a single barrier.

#### ACKNOWLEDGMENTS

The authors are grateful to M. Hauser for the MBE growth, and K. von Klitzing and H. Schneider for valuable discussions. Part of this work was sponsored by the Bundesministerium für Forschung und Technologie of the Federal Republic of Germany.

---

\*On leave from Nippon Telegraph and Telephone Corporation, Electrical Communication Laboratories, Tokyo 180, Japan.

<sup>1</sup>L. Esaki and R. Tsu, *IBM J. Res. Dev.* **14**, 61 (1970).

<sup>2</sup>R. A. Davis, M. J. Kelly, and T. M. Kerr, *Phys. Rev. Lett.* **55**, 1114 (1985).

<sup>3</sup>T. Nakagawa, H. Imamura, T. Sakamoto, K. Ohta, and N. J. Kawai, *Electron. Lett.* **21**, 882 (1985).

<sup>4</sup>L. Esaki and L. L. Chang, *Phys. Rev. Lett.* **33**, 495 (1974).

<sup>5</sup>R. F. Kazarinov and R. A. Suris, *Fiz. Tekh. Poluprovodn.* **5**, 797 (1971) [*Sov. Phys.—Semicond.* **5**, 707 (1971)].

<sup>6</sup>F. Capasso, K. Mohammed, and A. Y. Cho, *Appl. Phys. Lett.* **48**, 478 (1986).

<sup>7</sup>T. Furuta, K. Hirakawa, I. Yoshino, and H. Sakaki, *Jpn. J. Appl. Phys.* **25**, L151 (1986).

<sup>8</sup>Y. Masumoto, S. Tarucha, and H. Okamoto, *Phys. Rev. B* **33**, 5961 (1986).

<sup>9</sup>M. Tsuchiya, T. Matsusue, and H. Sakaki, *Phys. Rev. Lett.* **59**, 2356 (1987).

<sup>10</sup>S. Tarucha, K. Ploog, and K. von Klitzing, *Phys. Rev. B* **36**, 4558 (1987).

<sup>11</sup>Y. Masumoto, M. Matsuura, S. Tarucha, and H. Okamoto, *Phys. Rev. B* **32**, 4275 (1985).

<sup>12</sup>The calculation is carried out in the same way as reported in Ref. 10. A conduction-band-gap discontinuity of 1.0 eV and an electron effective mass in AlAs of  $0.15m_0^*$  are assumed.

<sup>13</sup>S. Hong and J. Singh, *Appl. Phys. Lett.* **49**, 331 (1986).

<sup>14</sup>R. T. Collins, K. von Klitzing, and K. Ploog, *Phys. Rev. B* **33**, 4378 (1986).

<sup>15</sup>J. D. Joannopoulos and G. Lucovsky, *The Physics of Hydrogen-generated Amorphous Silicon II* (Springer-Verlag, Berlin, 1984); M. A. Lampert and P. Mark, *Current Injection in Solids* (Academic, New York, 1970).

<sup>16</sup>H. J. Polland, K. Köhler, L. Schultheis, J. Kuhl, E. O. Göbel, and C. W. Tu, *Superlatt. Microstruct.* **2**, 309 (1986).

<sup>17</sup>E. L. Wolf, *Principles of Electron Tunneling Spectroscopy* (Oxford University Press, New York, 1985).